European Journal of Pharmaceutics and Biopharmaceutics 184 (2023) 7–15

Contents lists available at ScienceDirect

European Journal of Pharmaceutics and Biopharmaceutics

journal homepage: www.elsevier.com/locate/ejpb

Research paper

Simple preparation of POxylated nanomaterials for cancer chemo-PDT/PTT

Micaela Nave [a], Francisco J.P. Costa [a], Cátia G. Alves [a], Rita Lima-Sousa [a], Bruna L. Melo [a], Ilídio J. Correia [a,b,*], Duarte de Melo-Diogo [a,*]

[a] CICS-UBI – Centro de Investigação em Ciências da Saúde, Universidade da Beira Interior, 6200-506 Covilhã, Portugal
[b] CIEPQPF – Departamento de Engenharia Química, Universidade de Coimbra, 3030-790 Coimbra, Portugal

ARTICLE INFO

Keywords:
Combinatorial triple therapy
Light responsive nanoparticles
Multifunctional nanomaterials
Photodynamic therapy
Poly(2-ethyl-2-oxazoline)
Polymer-IR780 conjugate

ABSTRACT

Near infrared (NIR) light-responsive nanomaterials hold potential to mediate combinatorial therapies targeting several cancer hallmarks. When irradiated, these nanomaterials produce reactive oxygen species (photodynamic therapy) and/or a temperature increase (photothermal therapy). These events can damage cancer cells and trigger the release of drugs from the nanomaterials' core. However, engineering nanomaterials for cancer chemo-photodynamic/photothermal therapy is a complex process. First, nanomaterials with photothermal capacity are synthesized, being then loaded with photosensitizers plus chemotherapeutics, and, finally functionalized with polymers for achieving suitable biological properties. To overcome this limitation, in this work, a novel straightforward approach to attain NIR light-responsive nanosystems for cancer chemo-photodynamic/photothermal therapy was established. Such was accomplished by synthesizing poly(2-ethyl-2-oxazoline)-IR780 amphiphilic conjugates, which can be assembled into nanoparticles with photodynamic/photothermal capabilities that simultaneously encapsulate Doxorubicin (DOX/PEtOx-IR NPs). The DOX/PEtOx-IR NPs presented a suitable size and surface charge for cancer-related applications. When irradiated with NIR light, the DOX/PEtOx-IR NPs produced singlet oxygen as well as a smaller thermic effect that boosted the release of DOX by 1.7-times. In the *in vitro* studies, the combination of DOX/PEtOx-IR NPs and NIR light could completely ablate breast cancer cells (viability ≈ 4 %), demonstrating the enhanced outcome arising from the nanomaterials' chemo-photodynamic/photothermal therapy.

1. Introduction

The high complexity and heterogenicity of cancer have propelled the investigation of combinatorial approaches to tackle this disease [1]. This strategy aims to synergistically act on several cancer hallmarks through the use of chemotherapeutic drug combinations (or drugs plus ionizing radiation) [2,3]. Such combinations also open a route for an improved outcome due to their potential to bypass cancer resistance mechanisms and requirement for lower drug doses [2,4,5]. Nevertheless, the non-specificity of the enrolled agents is also a concern in this type of therapy [4–6]. In fact, the application of combinatorial cocktails in cancer therapy is challenging since it requires the management of multiple side-effects from the different entities [6].

In the last years, researchers and clinicians have been exploring the use of nanomaterials for mediating cancer combinatorial therapies. Nanomaterials can accommodate multiple agents (*e.g.*, drugs, essential oils) on their core/reservoirs, protecting them from degradation during circulation [7,8]. As importantly, the nanomaterials' physicochemical features (*e.g.*, size, surface composition) allow them to display an enhanced accumulation at the tumor site [9–12]. Such is of paramount importance to manage and reduce possible side-effects.

In this regard, nanomaterials with near infrared (NIR; 750 – 1000

Abbreviations: ANOVA, Analysis of Variance; CLSM, Confocal Laser Scanning Microscopy; DLS, Dynamic Light Scattering; DMEM-F12, Dulbecco's Modified Eagle's Medium F-12; DOX, Doxorubicin; DOX/PEtOx-IR NPs, Doxorubicin-loaded Poly(2-ethyl-2-oxazoline)-IR780 Nanoparticles; EE, Encapsulation Efficiency; FBS, Fetal Bovine Serum; FTIR, Fourier Transform Infrared Spectroscopy; ICG, Indocyanine green; MCF-7, Michigan Cancer Foundation-7 cellular lines; NHDF, Normal Human Dermal Fibroblasts; NIR, Near infrared; n.s., Non-significant; PBS, Phosphate Buffered Saline; PDI, Polydispersity Index; PDT, Photodynamic Therapy; PEG, Poly(ethylene glycol); PEtOx, Poly(2-ethyl-2-oxazoline); PEtOx-IR conjugate, Poly(2-ethyl-2-oxazoline)-IR780 conjugate; PEtOx-IR NPs, Poly(2-ethyl-oxazoline)-IR780 Nanoparticles; PEtOx-SH, Poly(2-ethyl-2-oxazoline) α-benzyl ω-thiol terminated; PTT, Photothermal Therapy; ROS, Reactive Oxygen Species; S.D., Standard Deviation; SOSG, Singlet Oxygen Sensor Green.

* Corresponding authors at: CICS-UBI – Centro de Investigação em Ciências da Saúde, Universidade da Beira Interior, 6200-506 Covilhã, Portugal (Ilídio J. Correia).
E-mail addresses: icorreia@ubi.pt (I.J. Correia), demelodiogo@fcsaude.ubi.pt (D. de Melo-Diogo).

https://doi.org/10.1016/j.ejpb.2023.01.009
Received 5 October 2022; Received in revised form 13 January 2023; Accepted 14 January 2023
Available online 20 January 2023

nm) light responsiveness are gathering a huge interest for anticancer applications owing to their potential for controlling the onset of the therapeutic effect [13]. In fact, the ability of these nanostructures to interact with NIR light is fundamental given the minimal interactions of this radiation with biological components (*e.g.*, water, melanin, hemoglobin), ensuring an appropriate penetration depth [11,14]. Upon interaction with NIR light, these nanostructures can produce reactive oxygen species (photodynamic therapy (PDT)) and/or a temperature increase (photothermal therapy (PTT)) [15]. These events not only cause direct damage to cancer cells but also increase cancer cells' sensitivity to chemotherapeutics' action [11,16]. In this way, combinatorial strategies based on nanomaterials' chemo-PDT/PTT hold a great potential to improve cancer treatment.

Despite their potential, engineering nanomaterials aimed for cancer chemo-PDT/PTT is a complex process. Generally, these multifunctional nanostructures are assembled by first synthesizing nanomaterials with photothermal capacity (*e.g.*, graphene derivatives, gold nanorods, Fe_3O_4 nanoclusters), which are subsequently loaded in their core/reservoirs with photosensitizers (*e.g.*, IR825, chlorin e6, RLP068) and chemotherapeutic drugs [17–21]. Subsequently, these nanostructures must be coated with hydrophilic non-fouling polymers (*e.g.*, poly(ethylene glycol) (PEG)) to increase their solubility and colloidal stability [22]. Importantly, this type of coating can also enhance the nanostructures' blood circulation time, which in turn increases their likelihood to accumulate in the tumor zone [23]. Therefore, these complex synthesis, assembly and functionalization processes hinder the scale-up and translation of the nanomaterials aimed for cancer chemo-PDT/PTT.

In this work, a novel and straightforward approach to attain a NIR light-responsive nanosystems for cancer chemo-PDT/PTT was established. Such was achieved by initially preparing a poly(2-ethyl-2-oxazoline)-IR780 conjugate (PEtOx-IR). This amphiphilic polymer contains IR780, a NIR light absorbing heptamethine cyanine with photodynamic and photothermal capabilities [4,24,25]. To produce the PEtOx-IR conjugate, the IR780′ cyclohexenyl ring was conjugated with the thiol-terminated poly(2-ethyl-2-oxazoline). This step not only aims to address the IR780′ weak water solubility and poor cytocompatibility but can also improve its biodistribution [22,26]. In fact, the coating of nanomaterials with poly(2-ethyl-2-oxazoline) can promote the nanostructures' tumor accumulation by prolonging their blood circulation time [27–29]. Poly(2-ethyl-2-oxazoline) has been deemed as a PEG alternative, which is important considering some immunogenicity cases reported for the latter [30].

Then, the synthesized amphiphilic PEtOx-IR conjugate was employed to prepare nanoparticles containing Doxorubicin through the nanoprecipitation technique (termed as DOX/PEtOx-IR NPs). To the best of our knowledge, the simple combination of PEtOx-IR and DOX for the preparation of nanomaterials aimed for cancer chemo-PDT/PTT has not yet been explored. The physicochemical, optical and *in vitro* biological properties of the produced nanoparticles were characterized to evaluate their suitability for cancer therapy.

2. Materials and methods

2.1. Materials

Doxorubicin (DOX) was acquired from Carbosynth (Berkshire, UK). IR780 Iodide, Poly(2-ethyl-2-oxazoline) α-benzyl ω-thiol terminated (PEtOx-SH; Mn = 10000 Da), Trypsin, Resazurin, Paraformaldehyde, and Dulbecco's Modified Eagle's Medium F-12 (DMEM-F12) were bought from Sigma-Aldrich (Sintra, Portugal). Acetone, Chloroform and Methanol were attained from Fisher Scientific (Oeiras, Portugal). Triethylamine and Hoechst 33342® were acquired from TCI (Oxford, UK) and Invitrogen (Massachusetts, USA), respectively. *T*-flasks, Cell Culture Plates, Calcein-AM, and Propidium Iodide (PI) were obtained from Thermo Fisher Scientific (Porto, Portugal). Normal Human Dermal Fibroblast (NHDF) and Michigan Cancer Foundation-7 (MCF-7) cell lines were obtained from Promocell (Heidelberg, Germany) and ATCC (Middlesex, UK), respectively. Fetal Bovine Serum (FBS) was purchased from Biochrom AG (Berlin, Germany). Singlet Oxygen Sensor Green (SOSG) was acquired from Thermo Fisher Scientific (Porto, Portugal). Cell Imaging Plates were bought from Ibidi GmbH (Munich, Germany). Double Deionized water (0.22 μm filtered, 18.2 M Ω cm) was used in all the assays.

2.2. Methods

2.2.1. Synthesis and Characterization of PEtOx-IR conjugate

The PEtOx-IR conjugate was synthesized by adapting previously published protocols [31,32]. In brief, PEtOx-SH (42 mg) was dissolved in chloroform (50 mL), followed by the addition of triethylamine (50 μL) and IR780 (64 mg). In this process, the PEtOx-SH was reacted with a molar excess of IR780 for 48 h at room temperature under stirring. Subsequently, the solvent was evaporated (Rotavap® R-215, Büchi, Switzerland) and the resulting product was resuspended in methanol. Afterwards, to remove the non-conjugated IR780, a dialysis against methanol was conducted (1 kDa molecular weight cut-off membrane) for 24 h at room temperature, culminating in the obtention of the PEtOx-IR conjugate. Fourier Transform Infrared Spectroscopy (FTIR; Nicolet iS10 spectrometer, Thermo Scientific Inc., MA, USA) was used to confirm the successful synthesis of PEtOx-IR conjugate.

2.2.2. Formulation and Characterization of DOX/PEtOx-IR NPs and PEtOx-IR NPs

The production of DOX/PEtOx-IR NPs was based on the nanoprecipitation technique previously reported by our group [33]. Initially, DOX (0.133 mg) and PEtOx-IR conjugate (0.653 mg) dissolved in methanol:acetone (2:3 (v/v); 1 mL) were added dropwise (0.3 mL h^{-1}) into Phosphate Buffered Saline (PBS; 5 mL) with uninterrupted stirring (200 rpm), at room temperature. After this step, the solution was dialyzed against water (0.5 – 1 kDa molecular weight cut-off membrane) during 90 min. Then, the recovered solution was centrifuged (17 460 *g*, 1 min), being the supernatant collected which contained the DOX/PEtOx-IR NPs. For the formulation of PEtOx-IR NPs, the same procedure was used without the addition of DOX.

The size distribution (in water) and the surface charge (in DMEM-F12 medium supplemented with 10 % (v/v) FBS) of DOX/PEtOx-IR NPs and PEtOx-IR NPs were evaluated by Dynamic Light Scattering (DLS) in a Zetasizer Nano ZS (Malvern Instruments ltd., Worcestershire, UK). Absorption spectroscopy (Evolution 201 spectrophotometer, Thermo Scientific Inc.) was used to determine the Encapsulation Efficiency of DOX in DOX/PEtOx-IR NPs. For such, the DOX/PEtOx-IR NPs were freeze-dried (in a ScanVac CoolSafe, LaboGene ApS, Lynge, Denmark) and resuspended in water:methanol (1:1 (v/v)). Then, the concentration of DOX was determined by verifying the samples' absorption at 498 nm and by using a standard curve of DOX (in water: methanol (1:1 (v/v), at 498 nm; the PEtOx-IR conjugate does not have absorbance at this wavelength in this solvent mixture)). Subsequently, the Encapsulation Efficiency was calculated using the following equation (1):

$$Encapsulation\ Efficiency(\%) = \frac{DOX\ weight\ incorpored\ in\ the\ nanoparticles}{DOX\ weight\ initially\ fed} \times 100 \quad (1)$$

Absorption spectroscopy was also employed to assess the ability of DOX/PEtOx-IR NPs and PEtOx-IR NPs to interact with NIR light. In this case, the absorption spectra of DOX/PEtOx-IR NPs and PEtOx-IR NPs (2.5 μg mL^{-1} of PEtOx-IR equivalents) in water were acquired.

2.2.3. Photodynamic and photothermal effect of DOX/PEtOx-IR NPs and PEtOx-IR NPs

The photodynamic and photothermal capabilities of the nanoformulations were characterized according to literature protocols [33–35]. To evaluate the photodynamic effect of DOX/PEtOx-IR NPs and PEtOx-IR NPs, the nanoformulations (at 2.5 and 12.5 μg mL^{-1} of PEtOx-IR) were mixed with SOSG (20 μL at 50 μM) and then were irradiated with NIR light (808 nm, 1.7 W cm^{-2}) during 5 min [34]. Then, the fluorescence of oxidized SOSG (λ_{ex} = 504 nm; λ_{em} = 530 nm) was measured in a spectrofluorometer (Spectramax Gemini EM spectrofluorometer, Molecular Devices LLC, CA, USA). Water (without nanoparticles) mixed with SOSG and exposed to NIR light was used as the control. For each condition, the blank was performed using the respective non-irradiated samples containing SOSG. The presence of DOX in DOX/PEtOx-IR NPs did not influence the fluorescence levels determined for oxidized SOSG.

On the other hand, to verify the photothermal capacity of DOX/PEtOx-IR NPs and PEtOx-IR NPs, these nanoformulations (at 2.5 and 12.5 μg mL^{-1} of PEtOx-IR equivalents) were exposed to NIR laser irradiation (808 nm, 1.7 W cm^{-2}) during 5 min [36]. The temperature variations were measured by using a thermocouple thermometer. In this assay, the temperature variation of irradiated water (without nanomaterials) was used as the control.

The procedure to evaluate the release of DOX from DOX/PEtOx-IR NPs was conducted as previously described by us [36]. For such, DOX/PEtOx-IR NPs in PBS (pH 7.4) were inserted in a membrane (0.5 – 1 kDa molecular weight cut-off) and dialyzed against PBS (pH 7.4) at 37 °C under constant stirring. At predetermined time points, samples were collected and analyzed by absorption spectroscopy to determine the DOX release. DOX/PEtOx-IR NPs were also exposed to NIR light at 4 h (808 nm, 1.7 W cm^{-2}, 5 min) to verify the influence of laser irradiation on DOX release.

2.2.4. Cytocompatibility evaluation of PEtOx-IR NPs

The cytocompatibility of PEtOx-IR NPs was evaluated in NHDF (normal cell line) and MCF-7 cells (breast cancer cell line) using the resazurin assay [37]. Initially, both cell lines (NHDF and MCF-7) were seeded (1×10^4 cells/well) in 96-well plates with DMEM-F12 medium supplemented with 10 % (v/v) FBS and 1 % (v/v) streptomycin/gentamycin, and, then placed in a humidified incubator (37 °C, 5 % CO_2). After 24 h, the medium was removed, and cells were incubated with PEtOx-IR NPs (at 1.25 and 2.5 μg mL^{-1} of PEtOx-IR equivalents) in fresh culture medium for 24 h or 48 h. Afterwards, the PEtOx-IR NPs were removed and resazurin in fresh culture medium (10 % (v/v)) was added to the cells, followed by 4 h of incubation in the dark (37 °C, 5 % CO_2). To verify the cells' viability, the resorufin fluorescence was measured in a spectrofluorometer (λ_{ex} = 560 nm; λ_{em} = 590 nm). Negative (K^-) and positive (K^+) controls were also performed using cells incubated only with fresh culture medium and with ethanol (70 % (v/v)), respectively.

2.2.5. Phototherapeutic effect of PEtOx-IR NPs and DOX/PEtOx-IR NPs towards MCF-7 cells

The phototherapeutic effect prompted by DOX/PEtOx-IR NPs and PEtOx-IR NPs towards breast cancer cells was evaluated through the resazurin assay [38,39]. Firstly, MCF-7 cells were seeded as indicated in Section 2.2.4. After one day, the medium was removed, and cells were incubated with DOX/PEtOx-IR NPs (at 1.88/1.25 and 3.76/2.5 μg mL^{-1} of DOX/PEtOx-IR conjugate equivalents) or PEtOx-IR NPs (at 1.25 and 2.5 μg mL^{-1} of PEtOx-IR conjugate equivalents) in fresh culture medium. After 4 h of incubation, the cells were irradiated with NIR light (808 nm, 1.7 W cm^{-2}, 5 min). After completing 24 h of incubation with the nanoformulations, the MCF-7 cells' viability was evaluated as mentioned in Section 2.2.4.

Confocal Laser Scanning Microscopy (CLSM; Zeiss LSM confocal microscope, Carl Zeiss AG, Oberkochen, Germany) was also used to visualize the phototherapeutic effect of both nanoformulations [36]. For such, MCF-7 cells were seeded (1.5×10^4 cells/well) in μ-slide 8-well imaging plates (Ibidi GmbH, Munich, Germany). After 48 h, MCF-7 cells were incubated with fresh medium containing DOX/PEtOx-IR NPs (3.76/2.5 μg mL^{-1} of DOX/PEtOx-IR conjugate equivalents) and PEtOx-IR NPs (2.5 μg mL^{-1} of PEtOx-IR conjugate equivalents). After 4 h of incubation, cells were irradiated with NIR light (808 nm, 1.7 W cm^{-2}, 5 min). Succeeding that, the medium was removed, and cells were stained with Calcein-AM/PI to label live/dead cells, according to the manufacturer's protocol. A $\lambda_{ex}/\lambda_{em}$ of 488/493–556 nm and 561/566–719 were used to visualize Calcein-AM and PI, respectively. MCF-7 cells just incubated with culture medium (without nanomaterials/NIR light) were used as the control for live cells.

2.2.6. Cellular uptake of DOX mediated by DOX/PEtOx-IR NPs

The cellular uptake of DOX mediated by DOX/PEtOx-IR NPs was assessed as previously described by our group [40]. In brief, MCF-7 cells were seeded and incubated with DOX/PEtOx-IR NPs (1.50/1 μg mL^{-1} of DOX/PEtOx-IR conjugate equivalents) as described in Section 2.2.4. MCF-7 cells were also exposed to NIR light (at 4 h post-incubation of the nanoparticles; 808 nm, 1.7 W cm^{-2}, 5 min). At specific time points (1, 6 and 24 h post-incubation of the nanoparticles), cells were washed with ice-cold Krebs Ringer Buffer for withdrawing the non-internalized DOX/PEtOx-IR NPs. Then, cells were exposed to a solution to cause their lysis (incubation with 1 % (v/v) of Triton X-100 in Krebs Buffer for 30 min under orbital stirring). By last, the DOX fluorescence ($\lambda_{ex}/\lambda_{em}$ of 480/570) was analyzed in a spectrofluorometer. Cells only exposed to Krebs Buffer were used as the control.

CLSM was also employed to evaluate the cellular uptake of DOX mediated by DOX/PEtOx-IR NPs. For such, MCF-7 cells were seeded in μ-slide 8-well imaging plates as described in Section 2.2.5. Afterwards, cells were incubated with fresh culture medium containing DOX/PEtOx-IR NPs (0.75/0.5 μg mL^{-1} of DOX/PEtOx-IR conjugate equivalents) for 24 h. At 4 h post-incubation of the nanoparticles, cells were also irradiated with NIR light (808 nm, 1.7 W cm^{-2}, 5 min). After the incubation periods, the medium was discarded, cells were washed with PBS and fixed with paraformaldehyde 4 % (w/v; 15 min, room temperature). Then, the cells' nucleus was stained with Hoechst 33342® (30 min, 4 °C). Fluorescence images were then acquired using a $\lambda_{ex}/\lambda_{em}$ of 405/410–499 (Hoechst 33342®) and 488/534–622 (DOX).

2.2.7. Statistical Analysis

To compare the different groups, a one-way Analysis of Variance (ANOVA) was applied with the Student-Newman-Keuls test. A value of p lower than 0.05 ($p < 0.05$) was considered statistically significant. To perform the data analysis, GraphPad Prism v7.0 (Trial version, GraphPad Software, CA, USA) was used.

3. Results and discussion

3.1. Formulation and Characterization of DOX/PEtOx-IR NPs and PEtOx-IR NPs

Classically, the preparation of nanomaterials aimed for cancer chemo-PDT/PTT is a laborious multi-step process, which has impact on their scalability and translatability. In order to overcome such problems, a PEtOx-IR conjugate was synthesized (its successful production was confirmed by FTIR; Fig. S1 and S2). Then, PEtOx-IR conjugate and DOX were used to formulate nanoparticles through the nanoprecipitation technique (termed as DOX/PEtOx-IR NPs) – Fig. 1A. This two-step approach was also applied to produce nanoparticles without DOX for comparison purposes (PEtOx-IR NPs).

After the production of the nanoparticles, their size was characterized by DLS (Fig. 1B). PEtOx-IR NPs revealed an average size of 196.0 ± 0.5 nm and a polydispersity index (PDI) of 0.178 ± 0.005 (n = 3; batch triplicates; Fig. 1B). Despite their average size, the PEtOx-IR NPs displayed a small population with a size of approximately 5038 nm,

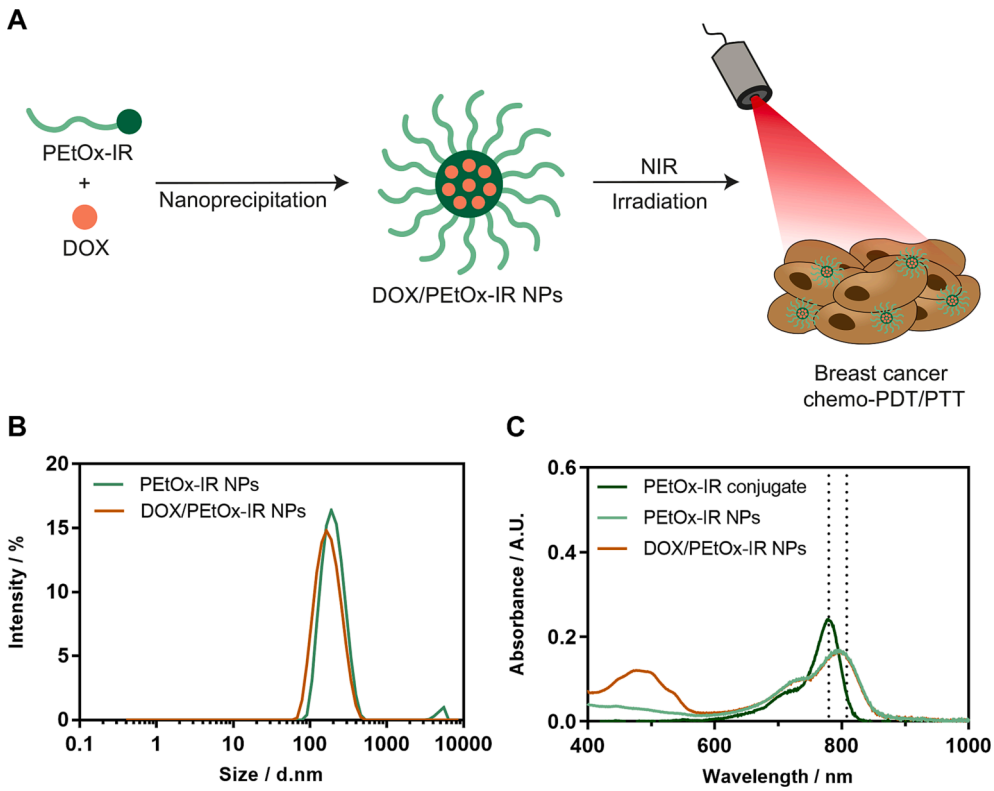

Fig. 1. Characterization of PEtOx-IR NPs and DOX/PEtOx-IR NPs physicochemical and optical properties. Schematic illustration of DOX/PEtOx-IR NPs application in cancer chemo-PDT/PTT (A). DLS size distribution of PEtOx-IR NPs and DOX/PEtOx-IR NPs (B). Absorption spectra of PEtOx-IR conjugate (at 2.5 μg mL^{-1}, in water: methanol (1:1 (v/v))), and of PEtOx-IR NPs and DOX/PEtOx-IR NPs (at 2.5 μg mL^{-1} of PEtOx-IR conjugate equivalents, in water) (C).

indicating that these nanostructures interact with each other or that present micro-sized aggregates. Interestingly, through the encapsulation of DOX, the nanostructures' size distribution was greatly improved (Fig. 1B). In fact, the DOX/PEtOx-IR NPs presented an average size of 160.7 ± 3.6 nm and a PDI of 0.125 ± 0.007 (n = 3; batch triplicates; Fig. 1B). The DOX/PEtOx-IR NPs showed not only a smaller size but also a unique size distribution without aggregates. Such behavior could be attributed to greater hydrophobic interactions occurring between IR780 (present in the PEtOx-IR conjugate) and DOX in the core of DOX/PEtOx-IR NPs, which improved the size distribution of this formulation when compared to PEtOx-IR NPs (formulation without DOX) [41]. The DOX/PEtOx-IR NPs' size distribution is also within the range (100 – 200 nm) considered to be optimal for passive targeting to the tumor zone through the enhanced permeability and retention effect [11].

The nanoparticles' zeta potential was also measured, being − 8.7 ± 1.6 mV and − 9.1 ± 0.3 mV for PEtOx-IR NPs and DOX/PEtOx-IR NPs, respectively. In this regard, both formulations presented a surface charge within the optimal range for application in cancer therapy (- 10 mV to + 10 mV), which is consistent with what it has been previously reported for PEtOx-coated nanomaterials [42,43].

The DOX/PEtOx-IR NPs could also successfully encapsulate DOX with an efficiency of about 63 ± 4 %. For instance, Alves *et al.* and Deng *et al.* produced nanoparticles encapsulating IR780 and DOX that presented a DOX encapsulation efficiency of about 20 % and 14 %, respectively [36,44]. The DOX/PEtOx-IR presented a higher DOX encapsulation efficiency, further confirming the importance of the hydrophobic interactions occurring between DOX and the PEtOx-IR conjugate in the nanoparticles' properties [36].

Then, the NIR absorption of PEtOx-IR NPs and DOX/PEtOx-IR NPs (2.5 μg mL^{-1} of PEtOx-IR conjugate) was evaluated (Fig. 1C). In this regard, PEtOx-IR NPs and DOX/PEtOx-IR NPs presented absorption peaks at 791 and 792 nm, respectively (Fig. 1C). As control, the absorption of the PEtOx-IR conjugate (dissolved in water:methanol (1:1 (v/v))) was also analyzed, revealing a maximum absorption peak at 781 nm (Fig. 1C). Due to this red-shift in the PEtOx-IR absorption when assembled in nanostructures, the PEtOx-IR NPs and DOX/PEtOx-IR NPs showed around 2.4-times higher absorption at 808 nm than the PEtOx-IR conjugate. This behavior could be correlated with the hydrophobic interactions occurring in the nanoparticles' core and/or with changes in the solvents' polarity [36,41]. The enhanced absorption at 808 nm displayed by PEtOx-IR NPs and DOX/PEtOx-IR NPs is of utmost importance since 808 nm laser light will be employed in the photodynamic/photothermal experiments, opening a venue for improved effects.

3.2. *Photodynamic and photothermal effects of DOX/PEtOx-IR NPs and PEtOx-IR NPs and NIR-enhanced DOX release*

After confirming the NIR absorption of PEtOx-IR NPs and DOX/PEtOx-IR NPs, their photodynamic and photothermal capabilities were evaluated. Initially, the photodynamic effect mediated by both formulations was investigated by using SOSG (Fig. 2A and 2B). For such, the PEtOx-IR NPs and DOX/PEtOx-IR NPs with SOSG were irradiated with NIR light (808 nm, 1.7 W cm^{-2}, 5 min), and then the fluorescence of oxidized SOSG was evaluated (SOSG becomes oxidized in the presence of singlet oxygen, being this change proportional to its fluorescence levels).

In this regard, the fluorescence of oxidized SOSG rose to 211 and 316 a.u. upon interaction with DOX/PEtOx-IR NPs plus NIR light and PEtOx-IR NPs plus NIR light, respectively, both at 2.5 μg mL^{-1} (of PEtOx-IR conjugate equivalents) - Fig. 2A and 2B. In stark contrast, the fluorescence levels of oxidized SOSG attained for water exposed to NIR light (50 a.u.; control) were about 4.2–6.3 times inferior (Fig. 2A and 2B). A greater dose of DOX/PEtOx-IR NPs and PEtOx-IR NPs (12.5 μg mL^{-1} of PEtOx-IR conjugate equivalents) in conjugation with NIR light could further increase the fluorescence of oxidized SOSG to 565 and 774 a.u.,

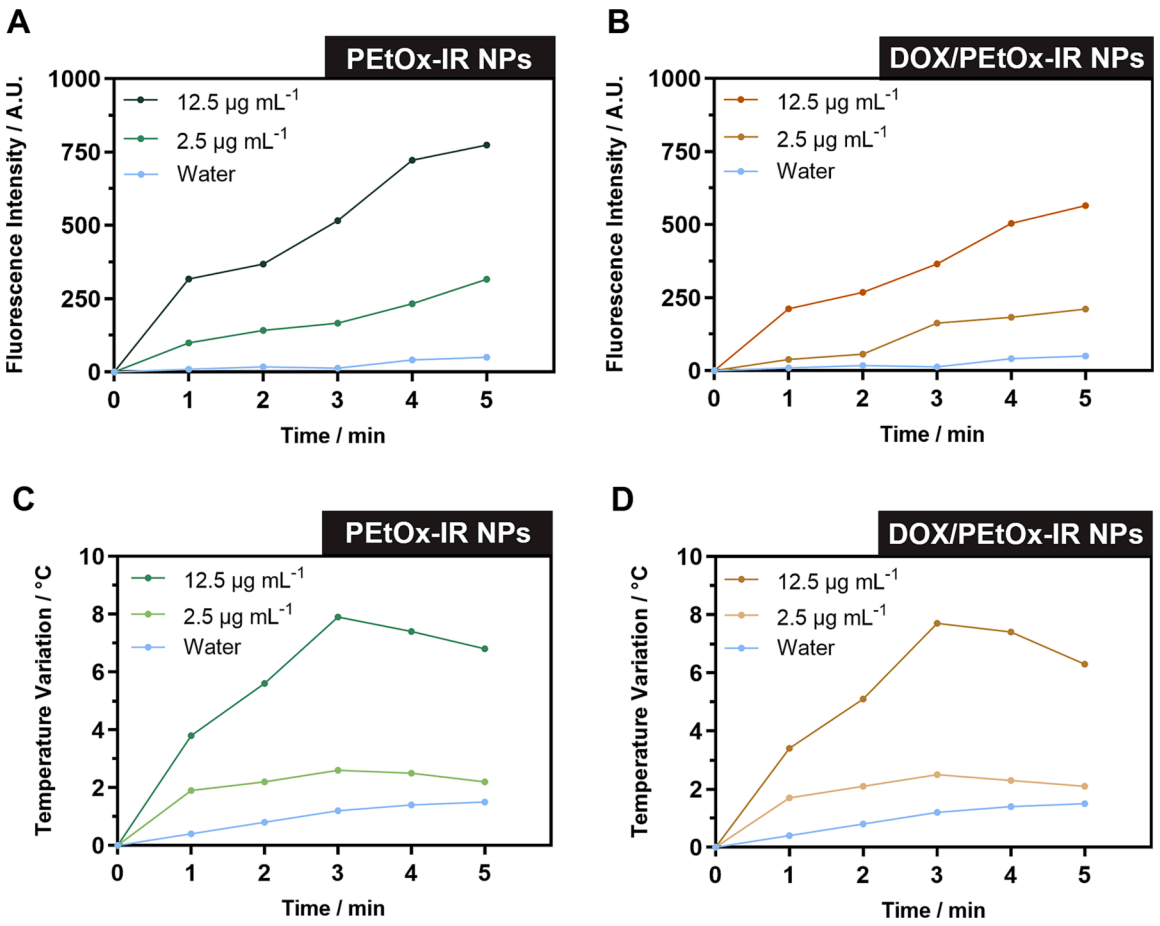

Fig. 2. Photodynamic and photothermal effect of PEtOx-IR NPs and DOX/PEtOx-IR NPs (at different concentrations of PEtOx-IR conjugate equivalents). Fluorescence intensity of oxidized SOSG ($\lambda_{ex}/\lambda_{em}$ = 504/530 nm) after interaction with PEtOx-IR NPs (A) and DOX/PEtOx-IR NPs (B) in conjugation with NIR light (808 nm, 1.7 W cm^{-2}). Temperature variation mediated by PEtOx-IR NPs (C) and DOX/PEtOx NPs (D) upon exposure to NIR light (808 nm, 1.7 W cm^{-2}).

respectively, being 11.3–15.5 times higher than those obtained for water plus NIR light (Fig. 2A and 2B). In fact, the ability of IR780-loaded nanomaterials to produce singlet oxygen upon NIR laser irradiation was previously demonstrated in some works [35,45]. Herein, the PEtOx-IR NPs and DOX/PEtOx-IR NPs, which are assembled using a novel PEtOx-IR conjugate developed by our group, also showed the ability to produce singlet oxygen upon NIR laser exposure, hence confirming their photodynamic potential.

To evaluate the photothermal capacity of PEtOx-IR NPs and DOX/PEtOx-IR NPs, these were irradiated with NIR light (808 nm, 1.7 W cm^{-2}, 5 min) and the temperature variations were monitored (Fig. 2C and 2D). For instance, at the lowest concentration tested (2.5 μg mL^{-1} of PEtOx-IR conjugate equivalents), the PEtOx-IR NPs and DOX/PEtOx-IR NPs generated, after 3 min of NIR laser irradiation, maximum temperature increases (ΔT) of 2.6 °C and 2.5 °C, respectively (Fig. 2C and 2D). After this time point, the attained photoinduced heat started to decrease. This behavior is likely to be correlated with the photodegradation of the PEtOx-IR conjugate present on the produced nanostructures since such phenomenon has been widely reported for IR780-loaded nanostructures [36,46]. On the other hand, water exposed to NIR light suffered a temperature increase of 1.2 °C and 1.5 °C after 3 and 5 min of NIR laser irradiation (Fig. 2C and 2D). Analyzing the 5th min of NIR laser exposure, the PEtOx-IR NPs and DOX/PEtOx-IR NPs at the dose of 2.5 μg mL^{-1} (of PEtOx-IR conjugate equivalents) produced a photoinduced heat that was just 1.4–1.5 times greater than that attained for the control (water plus NIR light). Exposing a higher concentration of DOX/PEtOx-IR NPs and PEtOx-IR NPs (12.5 μg mL^{-1} of PEtOx-IR conjugate equivalents) to 5 min of NIR light led to a final temperature variation of 6.3 and 6.8 °C, respectively, being 4.2–4.5 times higher than that of the control (Fig. 2C and 2D). Although the PEtOx-IR NPs and DOX/PEtOx-IR NPs could produce a higher photoinduced heat than the control, their photothermal capacity was not very high, highlighting that the photodynamic pathway is likely the dominant mechanism.

Nevertheless, we hypothesized that the nanostructures' photoinduced heat could still influence the release of DOX from the DOX/PEtOx-IR NPs. For such, the cumulative release of DOX from DOX/PEtOx-IR NPs was investigated in the absence and presence of NIR light (Fig. S4). After the NIR laser exposure (at 4 h), the release of DOX from the DOX/PEtOx-IR NPs greatly increased (Fig. S4). For instance, at the endpoint of the study, the non-irradiated nanoformulations had a 33 % DOX release, while those exposed to NIR light released 55 % of their cargo (Fig. S4). In this way, the NIR-laser exposure could increase the release of DOX from the DOX/PEtOx-IR NPs by up to 1.7-fold (Fig. S4). Altogether, these results confirm the good NIR responsiveness of the developed formulations.

3.3. Cytocompatibility of PEtOx-IR NPs

In order to verify the cytocompatibility profile of the PEtOx-IR NPs, these nanostructures were incubated in NHDF and MCF-7 cells, which were used as models of healthy and breast cancer cells, respectively (Fig. 3). NHDF exposed to PEtOx-IR NPs for 24 h and 48 h revealed a cell viability > 87 %, even at the highest concentration tested (2.5 μg mL^{-1} of PEtOx-IR conjugate equivalents) – Fig. 3A. In turn, MCF-7 cells exposed to PEtOx-IR NPs demonstrated a slight reduction on their viability over time (Fig. 3B). In this regard, MCF-7 cells remained with a

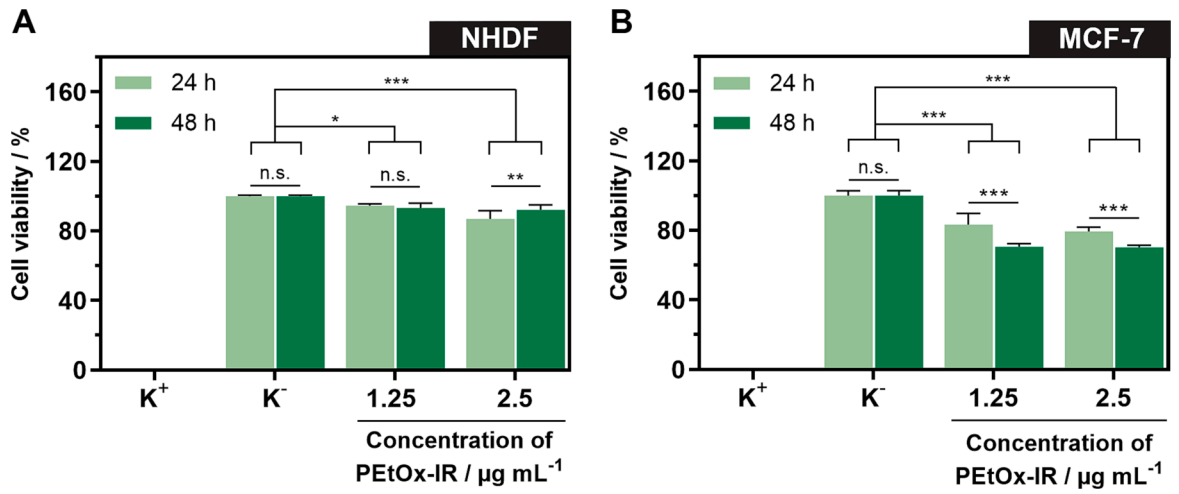

Fig. 3. Determination of PEtOx-IR NPs cytocompatibility. Viability of NHDF (A) and MCF-7 cells (B) after incubation with PEtOx-IR NPs (at 1.25 and 2.5 μg mL^{-1} of PEtOx-IR conjugate equivalents) for 24 and 48 h. K^+ and K^- represent the positive and negative controls, respectively. Each bar represents the mean ± S.D. n = 5 (*$p < 0.01$, **$p < 0.001$, ***$p < 0.0001$), n.s. = non-significant.

viability of 79 % after an incubation period of 24 h with this formulation (at 2.5 μg mL^{-1} of PEtOx-IR conjugate equivalents) - Fig. 3B. An incubation period of 48 h decreased slightly the MCF-7 cells' viability to about 70 % (Fig. 3B). This differential effect of PEtOx-IR NPs in NHDF and MCF-7 cells can be explained by the IR780 inherent cytotoxicity towards cancer cells due to its accumulation in their mitochondria [47]. In fact, this behavior has also been observed in other research works that used IR780-loaded nanomaterials for cancer therapy [33,48]. Nevertheless, the data obtained in NHDF is indicative that PEtOx-IR NPs display a good cytocompatibility towards healthy cells.

3.4. Phototherapeutic effect of DOX/PEtOx-IR NPs and PEtOx-IR NPs towards MCF-7 cells

Finally, the phototherapeutic effect of both nanoparticles was evaluated in MCF-7 cells. For such, the breast cancer cells were incubated with PEtOx-IR NPs and DOX/PEtOx-IR NPs, being after 4 h exposed to NIR light (808 nm, 1.7 W cm^{-2}, 5 min) – Fig. 4A. At the concentration of 1.25 μg mL^{-1} (of PEtOx-IR conjugate equivalents), the PEtOx-IR NPs did not affect meaningfully the MCF-7 cells (viability > 83 %), while PEtOx-IR NPs combined with NIR light could reduce the cells' viability to about 55 % (Fig. 4B). MCF-7 cells incubated with a greater concentration of PEtOx-IR NPs (2.5 μg mL^{-1} of PEtOx-IR conjugate equivalents) also revealed a high viability (> 79 %) - Fig. 4B. However, this dose of PEtOx-IR NPs combined with NIR light reduced the MCF-7 cells' viability to just 21 % (Fig. 4B). As importantly, the MCF-7 cells only exposed to NIR light did not reveal any signs of nefarious effects (viability ≈ 100 %) - Fig. 4B. Taken together, these results demonstrate that the on-demand outcome achieved by PEtOx-IR NPs combined with NIR light is related to the nanostructures' photodynamic/photothermal capabilities (Fig. 2A and 2C).

On the other hand, the DOX/PEtOx-IR NPs reduced the viability of the MCF-7 cells to 68 % and 17 % at the concentrations of 1.88/1.25 μg mL^{-1} and 3.76/2.5 μg mL^{-1} of DOX/PEtOx-IR conjugate equivalents, respectively (Fig. 4B). Since the PEtOx-IR NPs (without NIR light) barely influenced the viability of the breast cancer cells, this therapeutic outcome mediated by the DOX/PEtOx-IR NPs (without NIR light) can be attributed to the chemotherapeutic action of DOX. Interestingly, the combined action of DOX/PEtOx-IR NPs and NIR light could reduce the viability of the cancer cells to just 29 %, at an ultra-low dose of 1.88/1.25 μg mL^{-1} of DOX/PEtOx-IR conjugate equivalents (Fig. 4B). The total ablation of the breast cancer cells (viability ≈ 4 %) was achieved by using a higher dose of this nanoformulation (3.76/2.5 μg mL^{-1} of DOX/PEtOx-IR conjugate equivalents) combined with NIR light. The superior therapeutic efficacy of the DOX/PEtOx-IR NPs plus NIR light regimen can be attributed to its multimodal capabilities (chemo-PDT/PTT) as well as to its ability to mediate a NIR light-enhanced DOX uptake by MCF-7 cells (Fig. S5). In fact, the interaction of DOX/PEtOx-IR NPs with NIR light could increase the intracellular levels of DOX by up to 2.3-fold (Fig. S5). This NIR-light enhanced DOX uptake (mediated by DOX/PEtOx-IR NPs) was also visualized by CLSM (Fig. S6).

To confirm the therapeutic efficacy results, the MCF-7 cells exposed to the different treatments were also stained with Calcein-AM (labels live cells) and PI (labels dead cells), being then imaged by CLSM (Fig. 4C and 4D). In concomitance with the cell viability results, only Calcein-AM fluorescence signals were detected for breast cancer cells exposed to NIR light (Fig. 4D). The majority of the cancer cells incubated with PEtOx-IR NPs also displayed fluorescence from Calcein-AM (Fig. 4C). In turn, Calcein-AM and PI-stained cancer cells were imaged on the groups incubated with DOX/PEtOx-IR NPs and PEtOx-IR NPs plus NIR light (Fig. 4C and 4D). In contrast, only PI fluorescence signals were observed on the cancer cells exposed to DOX/PEtOx-IR NPs plus NIR light (Fig. 4D), which confirms with ablative capacity arising from the nanostructures' chemo-PDT/PTT.

Xu *et al.* synthesized gold nanorods (photothermal agent; 20 μg mL^{-1}), that were coated with PEG and loaded with a protoporphyrin IX derivative (photodynamic agent; 3.20 μg mL^{-1}) and DOX (2.10 μg mL^{-1}), that after exposure to 808 nm (1.0 W cm^{-2}, 5 min) and 635 nm (0.5 W cm^{-2}, 5 min) radiations, could decrease MCF-7 cells viability to 37 % [49]. Cheng team produced bovine serum albumin nanoparticles loaded with DOX (6.5 μg mL^{-1}) and ICG (photothermal and photodynamic agent; 13 μg mL^{-1}), that were complexed with AS1411 (targeting aptamer) and KALA (cell-penetrating peptide), verifying their capacity to decrease cancer cells' viability to about 20 % after exposure to NIR light (808 nm, 1.0 W cm^{-2}, 4 min) [50]. Wo *et al.* developed silica-coated hollow magnetic nanospheres (photothermal agent; 500 μg mL^{-1}) as well as carboxylated graphene quantum dots (photodynamic agent; 200 μg mL^{-1}), which together with DOX (300 μg mL^{-1}), were loaded into a liposome that could reduce the viability of cancer cells to approximately 15 % upon laser exposure (671 nm, 0.2 W cm^{-2}, 20 min) [51]. In this work, the DOX/PEtOx-IR NPs were prepared using a straightforward route and their combination with NIR light (3.76/2.5 μg mL^{-1} of DOX/PEtOx-IR conjugate equivalents; 808 nm, 1.7 W cm^{-2}, 5 min) could prompt the complete ablation of breast cancer cells, highlighting the simplicity and chemo-PDT/PTT potential of this nanosystem.

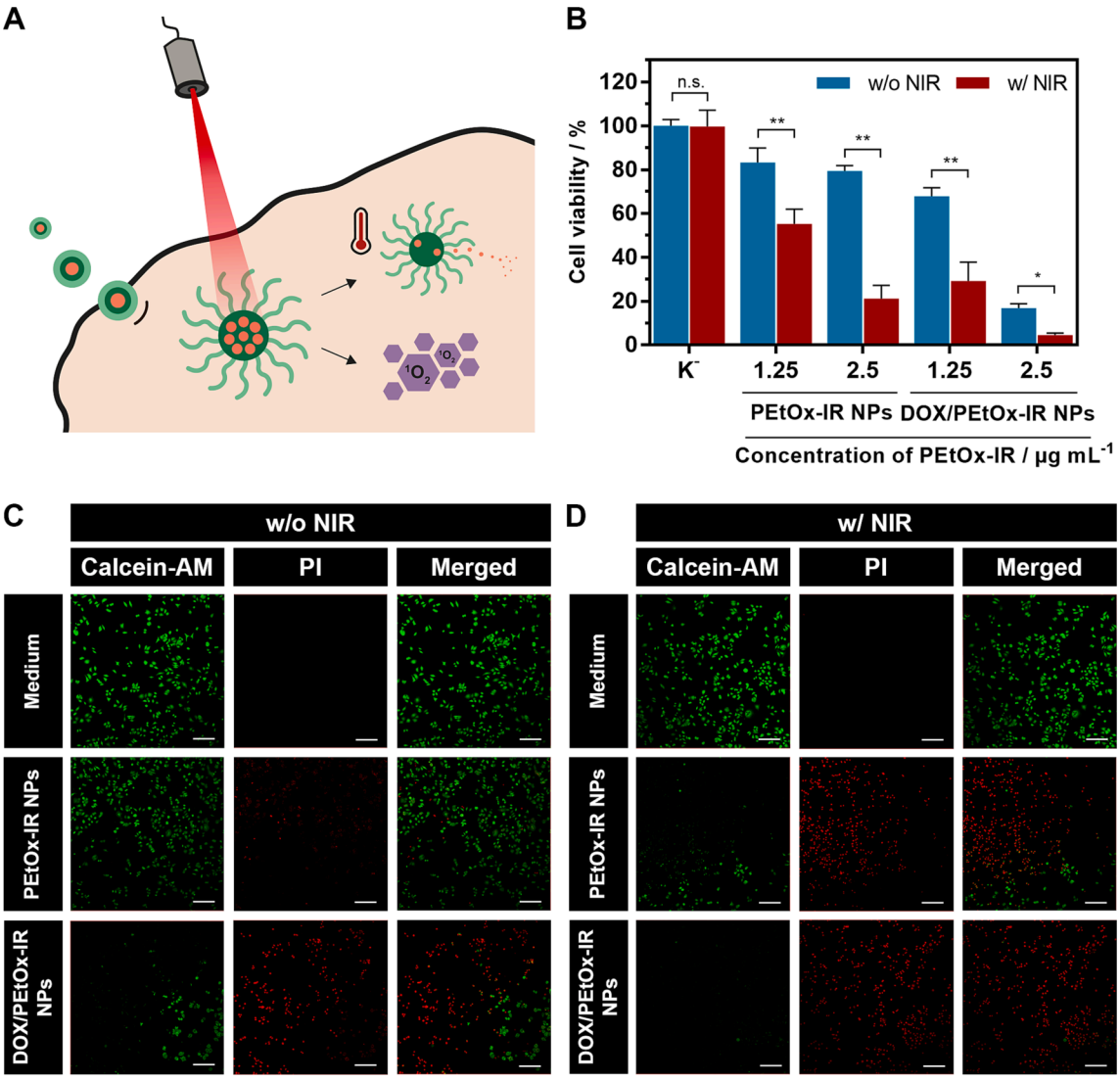

Fig. 4. Schematic representation of the DOX/PEtOx-IR NPs' action after NIR laser exposure (A). Cell viability of MCF-7 cells after incubation with PEtOx-IR NPs (at 1.25 and 2.5 μg mL^{-1} of PEtOx-IR conjugate equivalents) and DOX/PEtOx-IR NPs (at 1.88/1.25 and 3.76/2.5 μg mL^{-1} of DOX/PEtOx-IR conjugate equivalents) without NIR light (w/o NIR) and with NIR light exposure (w/ NIR; 808 nm, 1.7 W cm^{-2}, 5 min) (B). K^- w/o NIR represents the negative control, and K^- w/ NIR corresponds to MCF-7 cells solely irradiated with NIR light. Data represents mean ± S.D. n = 5 (*$p < 0.01$, **$p < 0.0001$), n.s. = non-significant. CLSM images of MCF-7 cells stained with Calcein-AM/PI after incubation with PEtOx-IR NPs (2.5 μg mL^{-1} of PEtOx-IR conjugate equivalents) and DOX/PEtOx-IR NPs (3.76/2.5 μg mL^{-1} of DOX/PEtOx-IR conjugate equivalents) w/o (C) and w/ NIR (D) laser irradiation (808 nm, 1.7 W cm^{-2}, 5 min). Medium w/o NIR corresponds to the control for live cells. Medium w/ NIR corresponds to cells only exposed to NIR light. Green channel: Calcein-AM; Red channel: PI. Scale bars represent 200 μm. (For interpretation of the references to colour in this figure legend, the reader is referred to the web version of this article.)

4. Conclusion

In this work, a novel and straightforward approach to attain NIR light-responsive nanosystems for cancer chemo-PDT/PTT was established. Such was accomplished by preparing PEtOx-IR conjugates, which can be assembled into nanoparticles with photodynamic/photothermal capabilities that simultaneously encapsulate DOX (DOX/PEtOx-IR NPs). The results revealed that the DOX/PEtOx-IR NPs present a suitable size (160.7 ± 0.5 nm), dispersity (0.178 ± 0.005) and surface charge (- 9.1 ± 0.3 mV) for cancer-related applications. The DOX/PEtOx-IR NPs could also successfully encapsulate DOX with an efficiency of about 63 ± 4 %. Compared to the PEtOx-IR conjugate, the DOX/PEtOx-IR NPs showed approximately 2.4-fold higher NIR absorption (at 808 nm). Upon interaction with this radiation, the DOX/PEtOx-IR NPs produced singlet oxygen (PDT) as well as a smaller thermic effect (PTT) that boosted the release of DOX by up to 1.7-times. In *in vitro* studies, the PEtOx-IR NPs (formulations without DOX) revealed a good cytocompatibility profile towards healthy and breast cancer cells. In turn, when the cancer cells were exposed to PEtOx-IR NPs plus NIR light (nanomaterials' PDT-PTT) and DOX/PEtOx-IR NPs (nanomaterials' chemotherapy), their viability decreased to 21 and 17 %, respectively. In contrast, the combination of DOX/PEtOx-IR NPs and NIR light led to the complete ablation of the breast cancer cells (viability ≈ 4 %), demonstrating the enhanced therapeutic outcome arising from the nanomaterials' chemo-PDT/PTT. In the future, *in vivo* assays will be crucial to fully depict the biocompatibility and chemo-PDT/PTT capacity of DOX/PEtOx-IR NPs.

Declaration of Competing Interest

The authors declare that they have no known competing financial interests or personal relationships that could have appeared to influence the work reported in this paper.

Data availability

Data will be made available on request.

Acknowledgements

This work was developed within the scope of the CICS-UBI projects UIDB/00709/2020 and UIDP/00709/2020, financed by national funds through the Portuguese Foundation for Science and Technology/MCTES. The funding from POCI-01-0145-FEDER-031462, PTDC/BTA-BTA/0696/2020 and 2022.06320.PTDC is also acknowledged. Duarte de Melo-Diogo acknowledges Foundation for Science and Technology (FCT) for the financial support given through a Junior Researcher contract (2021.00590.CEECIND). Cátia G. Alves, Rita Lima-Sousa and Bruna L. Melo acknowledge funding from individual PhD fellowships from FCT (SFRH/BD/145386/2019, SFRH/BD/144922/2019 and 2021.06044.BD).

Appendix A. Supplementary material

Supplementary data to this article can be found online at https://doi.org/10.1016/j.ejpb.2023.01.009.

References

[1] D. Hanahan, Hallmarks of Cancer: New Dimensions, Cancer, Discovery 12 (2022) 31–46, https://doi.org/10.1158/2159-8290.CD-21-1059.
[2] J.Y. Choi, R.K. Thapa, C.S. Yong, J.O. Kim, Nanoparticle-based combination drug delivery systems for synergistic cancer treatment, J. Pharm. Invest. 46 (2016) 325–339, https://doi.org/10.1007/s40005-016-0252-1.
[3] K. Bhatia, Bhumika, A. Das, Combinatorial drug therapy in cancer-New insights, Life Sci. 258 (2020), 118134, https://doi.org/10.1016/j.lfs.2020.118134.
[4] C. Pais-Silva, D. de Melo-Diogo, I.J. Correia, IR780-loaded TPGS-TOS micelles for breast cancer photodynamic therapy, Eur. J. Pharm. Biopharm. 113 (2017) 108–117, https://doi.org/10.1016/j.ejpb.2017.01.002.
[5] A. Hak, V. Ravasaheb Shinde, A.K. Rengan, A review of advanced nanoformulations in phototherapy for cancer therapeutics, Photodiagn. Photodyn. Ther. 33 (2021), 102205, https://doi.org/10.1016/j.pdpdt.2021.102205.
[6] M.J. Jo, I.S. Jin, C.-W. Park, B.Y. Hwang, Y.B. Chung, J.-S. Kim, D.H. Shin, Revolutionizing technologies of nanomicelles for combinatorial anticancer drug delivery, Arch. Pharmacal Res. 43 (2020) 100–109, https://doi.org/10.1007/s12272-020-01215-4.
[7] D. Kalyane, N. Kumar, N. Anup, K. Rajpoot, R. Maheshwari, P. Sengupta, K. Kalia, R.K. Tekade, Recent advancements and future submissions of silica core-shell nanoparticles, Int. J. Pharm. 609 (2021), 121173, https://doi.org/10.1016/j.ijpharm.2021.121173.
[8] O.A. Attallah, A. Shetta, F. Elshishiny, W. Mamdouh, Essential oil loaded pectin/chitosan nanoparticles preparation and optimization via Box-Behnken design against MCF-7 breast cancer cell lines, RSC Adv. 10 (2020) 8703–8708, https://doi.org/10.1039/c9ra10204c.
[9] C.F. Rodrigues, C.G. Alves, R. Lima-Sousa, A.F. Moreira, D. de Melo-Diogo, I. J. Correia, in: Advances and Avenues in the Development of Novel Carriers for Bioactives and Biological Agents, Elsevier, 2020, pp. 283–316, https://doi.org/10.1016/B978-0-12-819666-3.00010-9.
[10] R. Zein, W. Sharrouf, K. Selting, Physical properties of nanoparticles that result in improved cancer targeting, J. Oncol. 2020 (2020) 1–16, https://doi.org/10.1155/2020/5194780.
[11] D. de Melo-Diogo, C. Pais-Silva, D.R. Dias, A.F. Moreira, I.J. Correia, Strategies to Improve Cancer Photothermal Therapy Mediated by Nanomaterials, Adv. Healthcare Mater. 6 (2017) 1700073, https://doi.org/10.1002/adhm.201700073.
[12] N. Hoshyar, S. Gray, H. Han, G. Bao, The effect of nanoparticle size on in vivo pharmacokinetics and cellular interaction, Nanomedicine 11 (2016) 673–692, https://doi.org/10.2217/nnm.16.5.
[13] A.Y. Rwei, W. Wang, D.S. Kohane, Photoresponsive nanoparticles for drug delivery, Nano Today 10 (2015) 451–467, https://doi.org/10.1016/j.nantod.2015.06.004.
[14] A.S. Gonçalves, C.F. Rodrigues, A.F. Moreira, I.J. Correia, Strategies to improve the photothermal capacity of gold-based nanomedicines, Acta Biomater. 116 (2020) 105–137, https://doi.org/10.1016/j.actbio.2020.09.008.
[15] F. Zhang, Q. Wu, H. Liu, NIR light-triggered nanomaterials-based prodrug activation towards cancer therapy, Wiley Interdiscip Rev.: Nanomed. Nanobiotechnol. 12 (2020), e1643, https://doi.org/10.1002/wnan.1643.
[16] A. Khan, N.K. Jain, M. Gandhi, R. Prasad, R. Srivastava, Photo-Triggered Nanomaterials for Cancer Theranostic Applications, Nano LIFE 11 (2021) 2130004, https://doi.org/10.1142/S1793984421300041.
[17] H. Abrahamse, M.R. Hamblin, New photosensitizers for photodynamic therapy, Biochem. J. 473 (2016) 347–364, https://doi.org/10.1042/bj20150942.
[18] L. Zou, H. Wang, B. He, L. Zeng, T. Tan, H. Cao, X. He, Z. Zhang, S. Guo, Y. Li, Current approaches of photothermal therapy in treating cancer metastasis with nanotherapeutics, Theranostics 6 (2016) 762–772, https://doi.org/10.7150/thno.14988.
[19] N. Fernandes, C.F. Rodrigues, A.F. Moreira, I.J. Correia, Overview of the application of inorganic nanomaterials in cancer photothermal therapy, Biomater. Sci. 8 (2020) 2990–3020, https://doi.org/10.1039/D0BM00222D.
[20] M. Lan, S. Zhao, W. Liu, C.-S. Lee, W. Zhang, P. Wang, Photosensitizers for Photodynamic Therapy, Adv. Healthcare Mater. 8 (2019) 1900132, https://doi.org/10.1002/adhm.201900132.
[21] X. Qin, Z. Wang, C. Guo, Y. Jin, Multi-responsive drug delivery nanoplatform for tumor-targeted synergistic photothermal/dynamic therapy and chemotherapy, New J. Chem. 44 (2020) 3593–3603, https://doi.org/10.1039/C9NJ05650E.
[22] C.G. Alves, R. Lima-Sousa, D. de Melo-Diogo, R.O. Louro, I.J. Correia, IR780 based nanomaterials for cancer imaging and photothermal, photodynamic and combinatorial therapies, Int. J. Pharm. 542 (2018) 164–175, https://doi.org/10.1016/j.ijpharm.2018.03.020.
[23] M.J. Mitchell, M.M. Billingsley, R.M. Haley, M.E. Wechsler, N.A. Peppas, R. Langer, Engineering precision nanoparticles for drug delivery, Nat. Rev. Drug Discovery 20 (2021) 101–124, https://doi.org/10.1038/s41573-020-0090-8.
[24] D. Gao, X. Guo, X. Zhang, S. Chen, Y. Wang, T. Chen, G. Huang, Y. Gao, Z. Tian, Z. Yang, Multifunctional phototheranostic nanomedicine for cancer imaging and treatment, Mater. Today Bio 5 (2020), 100035, https://doi.org/10.1016/j.mtbio.2019.100035.
[25] H.S. Jung, P. Verwilst, A. Sharma, J. Shin, J.L. Sessler, J.S. Kim, Organic molecule-based photothermal agents: an expanding photothermal therapy universe, Chem. Soc. Rev. 47 (2018) 2280–2297, https://doi.org/10.1039/C7CS00522A.
[26] Y. Chen, Z. Li, H. Wang, Y. Wang, H. Han, Q. Jin, J. Ji, IR-780 Loaded Phospholipid Mimicking Homopolymeric Micelles for Near-IR Imaging and Photothermal Therapy of Pancreatic Cancer, ACS Appl. Mater. Interfaces 8 (2016) 6852–6858, https://doi.org/10.1021/acsami.6b00251.
[27] C.A. Reis, C.F. Rodrigues, A.F. Moreira, T.A. Jacinto, P. Ferreira, I.J. Correia, Development of gold-core silica shell nanospheres coated with poly-2-ethyl-oxazoline and β-cyclodextrin aimed for cancer therapy, Mater. Sci. Eng. C 98 (2019) 960–968, https://doi.org/10.1016/j.msec.2019.01.068.
[28] O. Koshkina, D. Westmeier, T. Lang, C. Bantz, A. Hahlbrock, C. Würth, U. Resch-Genger, U. Braun, R. Thiermann, C. Weise, M. Eravci, B. Mohr, H. Schlaad, R. H. Stauber, D. Docter, A. Bertin, M. Maskos, Tuning the Surface of Nanoparticles: Impact of Poly(2-ethyl-2-oxazoline) on Protein Adsorption in Serum and Cellular Uptake, Macromol. Biosci. 16 (2016) 1287–1300, https://doi.org/10.1002/mabi.201600074.
[29] S. Gulyuz, D. Bayram, U.U. Ozkose, Z.B. Bolat, P. Kocak, O.M. Saka, B. Devrim, M. Parlak Khalily, D. Telci, F. Sahin, S. Özçubukçu, E. Sezer, M.A. Tasdelen, O. Alpturk, A. Bozkır, O. Yilmaz, Synthesis, biocompatibility and gene encapsulation of poly(2-Ethyl 2-Oxazoline)-dioleoyl phosphatidylethanolamine (PEtOx-DOPE) and post-modifications with peptides and fluorescent dye coumarin, Int. J. Polym. Mater. Polym. Biomater. 70 (2021) 981–993, https://doi.org/10.1080/00914037.2020.1767617.
[30] O. Sedlacek, V.R. de la Rosa, R. Hoogenboom, Poly(2-oxazoline)-protein conjugates, Eur. Polym. J. 120 (2019), 109246, https://doi.org/10.1016/j.eurpolymj.2019.109246.
[31] A. Yuan, X. Qiu, X. Tang, W. Liu, J. Wu, Y. Hu, Self-assembled PEG-IR-780-C13 micelle as a targeting, safe and highly-effective photothermal agent for in vivo imaging and cancer therapy, Biomaterials 51 (2015) 184–193, https://doi.org/10.1016/j.biomaterials.2015.01.069.
[32] N. Luo, J.K. Weber, S. Wang, B. Luan, H. Yue, X. Xi, J. Du, Z. Yang, W. Wei, R. Zhou, G. Ma, PEGylated graphene oxide elicits strong immunological responses despite surface passivation, Nat. Commun. 8 (2017) 14537, https://doi.org/10.1038/ncomms14537.
[33] C.G. Alves, D. de Melo-Diogo, R. Lima-Sousa, I.J. Correia, IR780 loaded sulfobetaine methacrylate-functionalized albumin nanoparticles aimed for enhanced breast cancer phototherapy, Int. J. Pharm. 582 (2020), 119346, https://doi.org/10.1016/j.ijpharm.2020.119346.
[34] C. Jiang, H. Cheng, A. Yuan, X. Tang, J. Wu, Y. Hu, Hydrophobic IR780 encapsulated in biodegradable human serum albumin nanoparticles for photothermal and photodynamic therapy, Acta Biomater 14 (2015) 61–69, https://doi.org/10.1016/j.actbio.2014.11.041.
[35] S. Ma, J. Zhou, Y. Zhang, B. Yang, Y. He, C. Tian, X. Xu, Z. Gu, An Oxygen Self-sufficient Fluorinated Nanoplatform for Relieved Tumor Hypoxia and Enhanced Photodynamic Therapy of Cancers, ACS Appl. Mater. Interfaces 11 (2019) 7731–7742, https://doi.org/10.1021/acsami.8b19840.
[36] C.G. Alves, D. de Melo-Diogo, R. Lima-Sousa, E.C. Costa, I.J. Correia, Hyaluronic acid functionalized nanoparticles loaded with IR780 and DOX for cancer chemo-phototherapy, Eur. J. Pharm. Biopharm. 137 (2019) 86–94, https://doi.org/10.1016/j.ejpb.2019.02.016.
[37] R. Lima-Sousa, D. de Melo-Diogo, C.G. Alves, E.C. Costa, P. Ferreira, R.O. Louro, I. J. Correia, Hyaluronic acid functionalized green reduced graphene oxide for targeted cancer photothermal therapy, Carbohydr. Polym. 200 (2018) 93–99, https://doi.org/10.1016/j.carbpol.2018.07.066.
[38] D. de Melo-Diogo, E.C. Costa, C.G. Alves, R. Lima-Sousa, P. Ferreira, R.O. Louro, I. J. Correia, POxylated graphene oxide nanomaterials for combination chemo-phototherapy of breast cancer cells, Eur. J. Pharm. Biopharm. 131 (2018) 162–169, https://doi.org/10.1016/j.ejpb.2018.08.008.
[39] Z. Deng, C. Fang, X. Ma, X. Li, Y.-J. Zeng, X. Peng, One Stone Two Birds: Zr-Fc Metal-Organic Framework Nanosheet for Synergistic Photothermal and

Chemodynamic Cancer Therapy, ACS Appl. Mater. Interfaces 12 (2020) 20321–20330, https://doi.org/10.1021/acsami.0c06648.
[40] I. Mó, C.G. Alves, D. de Melo-Diogo, R. Lima-Sousa, I.J. Correia, Assessing the combinatorial chemo-photothermal therapy mediated by Sulfobetaine Methacrylate-functionalized nanoparticles in 2D and 3D in vitro cancer models, Biotechnol. J. 15 (2020), 2000219, https://doi.org/10.1002/biot.202000219.
[41] Y. Tan, Y. Zhu, L. Wen, X. Yang, X. Liu, T. Meng, S. Dai, Y. Ping, H. Yuan, F. Hu, Mitochondria-Responsive Drug Release along with Heat Shock Mediated by Multifunctional Glycolipid Micelles for Precise Cancer Chemo-Phototherapy, Theranostics 9 (2019) 691–707, https://doi.org/10.7150/thno.31022.
[42] Y. Gao, Y. Zhou, L. Zhao, C. Zhang, Y. Li, J. Li, X. Li, Y. Liu, Enhanced antitumor efficacy by cyclic RGDyK-conjugated and paclitaxel-loaded pH-responsive polymeric micelles, Acta Biomater. 23 (2015) 127–135, https://doi.org/10.1016/j.actbio.2015.05.021.
[43] Z.B. Bolat, A.E. Nezir, B. Devrim, E. Zemheri, S. Gulyuz, U.U. Ozkose, O. Yilmaz, A. Bozkir, D. Telci, F. Sahin, Delivery of doxorubicin loaded P18 conjugated-poly (2-ethyl-oxazoline)-DOPE nanoliposomes for targeted therapy of breast cancer, Toxicol. Appl. Pharmacol. 428 (2021), 115671, https://doi.org/10.1016/j.taap.2021.115671.
[44] H. Deng, X. Zhao, L. Deng, J. Liu, A. Dong, Reactive oxygen species activated nanoparticles with tumor acidity internalization for precise anticancer therapy, J. Controlled Release 255 (2017) 142–153, https://doi.org/10.1016/j.jconrel.2017.04.002.
[45] D. Wang, S. Zhang, T. Zhang, G. Wan, B. Chen, Q. Xiong, J. Zhang, W. Zhang, Y. Wang, Pullulan-coated phospholipid and Pluronic F68 complex nanoparticles for carrying IR780 and paclitaxel to treat hepatocellular carcinoma by combining photothermal therapy/photodynamic therapy and chemotherapy, Int. J. Nanomed. 12 (2017) 8649–8670, https://doi.org/10.2147/ijn.s147591.
[46] G. Wan, Y. Cheng, J. Song, Q. Chen, B. Chen, Y. Liu, S. Ji, H. Chen, Y. Wang, Nucleus-targeting near-infrared nanoparticles based on TAT peptide-conjugated IR780 for photo-chemotherapy of breast cancer, Chem. Eng. J. 380 (2020), 122458, https://doi.org/10.1016/j.cej.2019.122458.
[47] R. Zhao, X. Ning, M. Wang, A. Yu, Y. Wang, A multifunctional nano-delivery system enhances the chemo-co-phototherapy of tumor multidrug resistance via mitochondrial-targeting and inhibiting P-glycoprotein-mediated efflux, J. Mater. Chem. B 9 (2021) 9174–9182, https://doi.org/10.1039/D1TB01658J.
[48] M. Chen, N. Bhattarai, M. Cong, R.L. Pérez, K.C. McDonough, I.M. Warner, Mitochondria targeting IR780-based nanoGUMBOS for enhanced selective toxicity towards cancer cells, RSC Adv. 8 (2018) 31700–31709, https://doi.org/10.1039/c8ra05484c.
[49] W. Xu, J. Qian, G. Hou, Y. Wang, J. Wang, T. Sun, L. Ji, A. Suo, Y. Yao, PEGylated hydrazided gold nanorods for pH-triggered chemo/photodynamic/photothermal triple therapy of breast cancer, Acta Biomater. 82 (2018) 171–183, https://doi.org/10.1016/j.actbio.2018.10.019.
[50] L. Xu, S.-B. Wang, C. Xu, D. Han, X.-H. Ren, X.-Z. Zhang, S.-X. Cheng, Multifunctional Albumin-Based Delivery System Generated by Programmed Assembly for Tumor-Targeted Multimodal Therapy and Imaging, ACS Appl. Mater. Interfaces 11 (2019) 38385–38394, https://doi.org/10.1021/acsami.9b11263.
[51] F. Wo, R. Xu, Y. Shao, Z. Zhang, M. Chu, D. Shi, S. Liu, A Multimodal System with Synergistic Effects of Magneto-Mechanical, Photothermal, Photodynamic and Chemo Therapies of Cancer in Graphene-Quantum Dot-Coated Hollow Magnetic Nanospheres, Theranostics 6 (2016) 485–500, https://doi.org/10.7150/thno.13411.